Wang, W.; Xu, X.; Li, Z.; Kratz, K.; Ma, N.; Lendlein, A.:
Modulating human mesenchymal stem cells using poly(Eta-butyl acrylate) networks in vitro with elasticity matching human arteries.
In: Clinical Hemorheology and Microcirculation. Vol. 71 (2019) 2, 277 - 289.
First published online by IOS: April 04, 2019

DOI: 10.3233/CH-189418
https://dx.doi.org/10.3233/CH-189418

Modulating human mesenchymal stem cells using poly(*n*-butyl acrylate) networks *in vitro* with elasticity matching human arteries

Weiwei Wang [1,#], Xun Xu [1,2,#], Zhengdong Li [1,2], Karl Kratz [1,3], Nan Ma [1,2,3,*] and Andreas Lendlein [1,2,3,4,*]

[1] Institute of Biomaterial Science and Berlin-Brandenburg Center for Regenerative Therapies, Helmholtz-Zentrum Geesthacht, 14513 Teltow, Germany

[2] Institute of Chemistry and Biochemistry, Freie Universität Berlin, 14195 Berlin, Germany

[3] Helmholtz Virtual Institute "Multifunctional Biomaterials for Medicine", 14513 Teltow, Germany

[4] Institute of Chemistry, University of Potsdam, 14476 Potsdam, Germany

# These authors contributed equally to this work.

* To whom correspondence should be addressed:

Prof. Dr. Nan Ma, Prof. Dr. Andreas Lendlein

Email: nan.ma@hzg.de, andreas.lendlein@hzg.de

Phone: +49 (0)3328 352 450

Fax: +49 (0)3328 352 452

Abstract

Non-swelling hydrophobic poly(*n*-butyl acrylate) network (cP*n*BA) is a candidate material for synthetic vascular grafts owing to its low toxicity and tailorable mechanical properties. Mesenchymal stem cells (MSCs) are an attractive cell type for accelerating

endothelialization because of their superior anti-thrombosis and immune modulatory function. Further, they can differentiate into smooth muscle cells or endothelial-like cells and secret pro-angiogenic factors such as vascular endothelial growth factor (VEGF). MSCs are sensitive to the substrate mechanical properties, with the alteration of their major cellular behavior and functions as a response to substrate elasticity. Here, we cultured human adipose-derived mesenchymal stem cells (hADSCs) on cP*n*BAs with different mechanical properties (cP*n*BA250, Young's modulus (E) = 250 kPa; cP*n*BA1100, E = 1100 kPa) matching the elasticity of native arteries, and investigated their cellular response to the materials including cell attachment, proliferation, viability, apoptosis, senescence and secretion. The cP*n*BA allowed high cell attachment and showed negligible cytotoxicity. F-actin assembly of hADSCs decreased on cP*n*BA films compared to classical tissue culture plate. The difference of cP*n*BA elasticity did not show dramatic effects on cell attachment, morphology, cytoskeleton assembly, apoptosis and senescence. Cells on cP*n*BA250, with lower proliferation rate, had significantly higher VEGF secretion activity. These results demonstrated that tuning polymer elasticity to regulate human stem cells might be a potential strategy for constructing stem cell-based artificial blood vessels.

Keywords: poly(*n*-butyl acrylate), mechanical property, vascular graft, mesenchymal stem cells, VEGF

1. Introduction

Artificial blood vessels are promising alternatives of allogeneic and autologous grafts for treating vascular diseases. The functionality of artificial blood vessels is highly dependent on the scaffold materials as well as their interacting cells [1-3]. The scaffold is required to be non-toxic and be able to support favorable cell attachment, differentiation and secretion of functional proteins. In addition, appropriate mechanical strength of the scaffold material is necessary to withstand the *in vivo* hemodynamic

forces. The reported poly(*n*-butyl acrylate) networks (cP*n*BAs) have demonstrated a high potential as synthetic vascular grafts [4]. The cP*n*BA polymers showed negligible cytotoxicity and could support the survival of cell lines as well as primary endothelial cells [4,5]. They also presented a high immuno-compatibility as demonstrated via the *in vitro* immune activation test [6]. Importantly, by varying the crosslinker content the elasticity of the cP*n*BA could be easily tailored to match the elasticity of native arteries, which varies in the range between 100 kPa and 1000 kPa [7-9].

Native blood vessels, aside from capillaries, consist of three layers. The endothelial cells (ECs) form the luminal side of the tunica intima and play a role to resist thrombosis and facilitate laminar flow of blood, and smooth muscle cells (SMCs) in the tunica media are responsible for remodeling of the vessel wall as well as stabilizing the elasticity and radial compliance of the vessel [1,10]. In order to mimic the structure and function of native vessels, several types of cells have been used for preparing artificial blood vessels, including ECs, SMCs, endothelial progenitor cells (EPCs), mesenchymal stem cells (MSCs) and embryonic stem cells (ESCs) [1,10,11]. Notably, MSCs have shown a high potential due to their intrinsic advantages such as abundance, self-renewal capacity, high proliferative potential and long-term viability. They could accelerate the process of endothelialization as they own the superior anti-thrombosis and immune modulatory functions. Importantly, they could differentiate into SMCs or endothelial-like cells and secret pro-angiogenic factors such as vascular endothelial growth factor (VEGF) to promote vascularization. Futher, MSCs share the similar origin as pericytes, which are contractile cells abundant in blood microvessels. Pericytes can interact with endothelial cells and modulate the stabilization and hemodynamics of vessels [12,13]. Therefore, pre-seeding of MSCs on a vascular graft *in vitro* may improve the function of the artificial blood vessels after implantation. In this case, the graft material should allow the favorable behaviors of MSCs including the high cell attachment, proliferation, survival and secretion of functional factors.

Accumulated evidences have proven the sensitivity of MSCs to their surrounding micro-environment. The cellular behavior and function of MSCs could be regulated by

various physical cues such as substrate mechanical property [14], surface topography [15] and external force [16] via the process termed mechanotransduction [17]. Among those, a lot of attention has been drawn to the cellular response of MSCs to substrate elasticity [18]. For example, the cell fate of MSCs has been shown to be influenced by matrix elasticity at the tissue level. The soft matrices (E = 0.1-1 kPa) mimicking brain tissue, stiffer matrices (8-17 kPa) mimicking muscle and more stiffer matrices (25-40 kPa) mimicking the crosslinked collagen of osteoids could lead to MSC neurogenesis, myogenesis and osteogenesis [19]. However, currently little is known about the MSC response to scaffold elasticity in the range matching the native arteries. In this study, we hypothesized that the favorable cellular behaviors of MSCs for constructing the stem cell-based artificial blood vessels could be achieved via tuning the scaffold elasticity in the range of arteries. We investigate two types of cP*n*BA films with different elastic moduli (E = 250 kPa for cP*n*BA250; 1100 kPa for cP*n*BA1100 at ambient temperature) as substrate materials for human adipose-derived mesenchymal stem cells (hADSCs). Tissue culture plate (TCP) was included as a reference material. The major cellular behaviors were assessed, including the early stage attachment, proliferation, actin cytoskeleton assembly, viability, apoptosis, cellular senescence, secretion of cytokines and cell migration.

2. Materials and Methods

2.1. cP*n*BA films

The cP*n*BA polymer networks were synthesized via bulk radical polymerization as described previously [4]. The solution containing *n*-butyl acrylate (*n*BA), poly(propylene glycol) dimethacrylate (PPGDMA) as crosslinker, and AIBN as initiator was filled into the molds formed by two glass plates and a 1.0 mm thick Teflon spacer for polymerization. The obtained polymer films were purified by swelling–deswelling in mixtures of *n*-hexane and chloroform, dried at 40 °C under vacuum, and sterilized using ethylene oxide (gas phase: 10 wt% ethylene oxide, 54 °C, 65% relative

humidity, 0.17 MPa, 3 h gas exposure time and 21 h aeration phase). The amount of crosslinker was changed to tailor the properties of the cP*n*BAs, which have been characterized in our previous study, including the polymer wettability evaluated via dynamic contact angle measurements, the surface profiles and roughness measured via optical profilometry as well as the mechanical properties determined by tensile tests at ambient temperature [4]. In this work, the substrates with Young's modulus of 250 ± 20 kPa (cP*n*BA250, 0.4 wt% PPGDMA) and 1110 ± 20 kPa (cP*n*BA1100, 7.3 wt% PPGDMA) were tested. To perform experiments with cells, the round-shaped cP*n*BA films with a diameter of 13 mm (Figure 1A) were put into the commercial standard 24-well TCP (Greiner Bio-One, Frickenhausen, Germany), which was made of polystyrene with modified surface for adherent cell culture. In parallel, the TCP without cP*n*BA films was used as a reference material.

2.2. Cell culture

The hADSCs were isolated from adipose tissue obtained by abdominal liposuction from a female donor after informed consent (No.: EA2/127/07; Ethics Committee of the Charité - Universitätsmedizin Berlin, approval from 17.10.2008) [20]. The fat tissue was dissociated for 60 minutes at 37 °C with collagenase NB4® (Serva GmbH, Heidelberg, Germany), followed by passing through a 100 µm cell strainer to remove the undissociated tissue. Then, the obtained cells were washed and cultured in a humidified atmosphere containing 5 vol% CO_2 at 37 °C. The non-attached cells were removed after 2 days and the attached cells were cultured in stem cell medium (MSCGM^{TM}, Lonza, Walkersville, MD, USA) without additional differentiation promoting factors. To maintain cell growth, the medium was changed every 3 days and the cells were passaged at a ratio of 1:3 when reaching ~90% confluence.

2.3. Cell adhesion and proliferation

The cells were seeded at a density of 1.0×10^4 cells/well. The early stage cell adhesion was evaluated via phase-contrast microscope after 24 hours. The cell proliferation rate was determined using a Cell Counting Kit-8 (CCK-8, Dojindo Molecular Technologies,

Munich, Germany). At the indicated time points, the old medium was replaced with 400 µl of fresh medium for each well, followed by addition of 40 µl of CCK-8 solution. After 2 hours of incubation at 37 °C, 110 µl of medium/CCK-8 mixture was transferred from each well into a transparent 96-well TCP. A microplate reader (Infinite 200 PRO®, Tecan Group Ltd., Männedorf, Switzerland) was used to measure the absorbance of the mixture at 450 nm and at a reference wavelength of 600 nm. Finally, the cell number was calculated using a standard curve, which was generated by measuring the absorbance value of a series of samples with known cell number.

2.4. Fluorescent staining

The cytoskeleton organization of the cells was studied after 2 weeks of culture on different materials. The fibrous actin (F-actin) stress fibers were stained with rhodamine conjugated phalloidin (Invitrogen, Paisley, UK) according to the given protocol. The cell nuclei were counterstained with 4',6-diamidino-2-phenylindole (DAPI). The cell viability was evaluated via a live/dead staining. After 2 weeks of culture on the materials, the cells were stained with fluorescein diacetate (FDA, 25 µg/ml) and propidium iodide (PI, 2 µg/mL) to identify the living and dead cells, respectively. After staining, the cells were washed with phosphate-buffered saline (PBS) buffer for three times, and the fluorescence images were obtained with a confocal laser scanning microscope (LSM 510 META, Carl Zeiss, Jena, Germany).

2.5. Apoptosis assay

The activation level of caspase-3/7 was detected to assess the cell apoptosis using an apoptosis kit (Caspase-Glo®, Promega, Madison, WI, USA) at day 1 and 7 after cell seeding. The old medium was first replaced with 240 µl of fresh culture medium for each well. Then, 200 µl of Caspase-Glo® 3/7 reagent was added and the mixture was shaken orbitally at 300 rpm for 30 seconds. Following an incubation at room temperature for 90 minutes, 200 µl of mixture was transferred from each well into a 96-well opaque (white) plate, and the luminescence intensity was measured using a

microplate reader (Infinite 200 PRO®, Tecan Group Ltd., Männedorf, Switzerland). The result was expressed as the relative light units (RLU) of the measured samples.

2.6. Cellular senescence assay

To measure the level of cellular senescence, the activity of the acidic senescence-associated ß-galactosidase (SA-ß-Gal) was examined at day 7 and 21 after cell seeding using a cellular senescence assay kit (Cell Biolabs, Inc., San Diego, CA, USA). The culture medium was carefully removed and the cells were washed 2 times with cold PBS. Then, 400 µl of lysis buffer was applied for each well and incubated at 4 °C for 5 minutes to lyse the cells. The obtained cell lysate was centrifuged for 10 minutes at 4 °C to collect the supernatant. Finally, the activity of SA-ß-Gal in the supernatant was determined with the fluorometric substrate according to the provided protocol. In addition, the total protein in the cell extract was quantified using a BCA protein assay kit (Thermo Fisher Scientific, Bonn, Germany). The result was expressed as the fluorescence intensity of the measured samples normalized with the amount of the total protein.

2.7. Cytokine secretion assay

The concentration of secreted inflammatory cytokines in the conditioned medium was measured. The conditioned media, derived from the fresh media added at day 0, 4, 11 an d 18 with the volume of 700 µl per well, were collected and stored at -20 °C at day 1, 7, 14 and 21. The concentration of the cytokines in the conditioned media were measured using a Bio-Plex® 200 system (BioRad, Munich, Germany) according to the manufacturer's instructions.

2.8. ELISA

The F-actin amount in cells on different materials was determined after 2 weeks of culture. Cells were first lysed and the F-actin concentration in the cell extract was measured using a human F-actin ELISA kit (Cusabio, Wuhan, Hubei, P. R. China). The amount of total protein in the cell extract was measured using the BCA protein assay kit (Thermo Fisher Scientific, Bonn, Germany). The result was expressed as the F-actin

level normalized with the total protein amount in the cell extract. The vascular endothelial growth factor (VEGF) protein in the conditioned medium was quantified using a human VEGFA ELISA kit (Thermo Fisher Scientific, Bonn, Germany) at day 1, 7, 14 and 21 respectively after cell seeding. The conditioned medium was collected as described above, and the cell number on the materials was quantified with CCK-8 (Dojindo Molecular Technologies, Munich, Germany). The result was expressed as VEGF level normalized with the cell number.

2.9. Cell migration

After 2 days of culture on different materials, the cell nuclei were stained with Hoechst 33342. Then, the cells were tracked for 24 hours using a time-lapse imaging microscope (IX81 motorized inverted microscope, Olympus, Hamburg, Germany), equipped with a bold line cage incubator to provide the humidified atmosphere (37 °C, 5 vol% CO_2) for supporting cell survival. To analyze the migration parameters, the obtained images were processed using ImageJ software (National Institutes of Health, USA) with the plug-ins "manual tracking" and "chemotaxis and migration tool" (ibidi GmbH, Martinsried, Germany).

2.10. Statistics

The number of replicates for experiments was indicated in the figure legend of the respective assays, and the quantification data were expressed as arithmetic mean ± standard deviation unless indicated otherwise. Statistical analysis was performed using one-way analysis of variance (ANOVA) with *post hoc* Tukey's test. A p value less than 0.05 was considered to be statistically significant.

3. Results and discussion

In this study, we prepared cP*n*BA films with different mechanical properties as substrate materials for hADSCs. In order to solely study the influence of the materials´ elasticity on cells, the used cP*n*BA films should have similar surface properties to avoid the influence of other aspects. Our previous study has demonstrated that the surface

properties are similar between these two types of cP*n*BA films, and remain constant after sterilization with ethylene oxide. The root mean square roughness R_q of sterilized samples was 1.0 ± 0.3 μm for cP*n*BA250 and 0.7 ± 0.2 μm for cP*n*BA1100, and the advancing contact angle was 116 ± 9° and 104 ± 5° respectively [4].

3.1. Cell adhesion and proliferation

A high cell adhesion rate onto the graft materials at the early stage is necessary for constructing artificial blood vessels with MSCs. This is of especial importance in the case that the cells were pre-cultured on the materials before implantation. After implantation, a tight attachment on the implants is required for cells to withstand the physiologic blood flow. In general, the cell adhesion could be improved by modifying the material surface such as coating with extra-cellular matrix (ECM) proteins. Here, the early stage cell adhesion was examined 24 hours after cell seeding. The cells could attach and spread on both cP*n*BA films even without ECM coating, showing typical spindle-shaped morphology similar to the cells on TCP (Figure 1B). The integrin is the primary cell membrane receptor to mediate the cell-material interaction and perceive various signals in the process of mechanotransduction [21]. Integrin activation could trigger a series of cellular responses including cell adhesion, cytoskeletal formation, gene expression and proliferation [22]. Therefore, allowing a high cell adhesion rate is one of the most important features of the materials used as vascular grafts.

The proliferation of MSCs could be regulated by material elasticity [18]. For example, mouse MSCs cultured on hydrogels with different elasticity (Young's moduli from 13 to 68 kPa) were found to proliferate faster on stiffer surface [23]. Similar results have also been observed in human MSCs cultured on hydrogels with different stiffness (storage moduli from 0.6-8.2 kPa) [24]. Here, our results suggested that the cells could even sense the difference of materials at the higher range of elasticity. The cells on cP*n*BA250 presented slower cell proliferation rate than on cP*n*BA1100. After 3 weeks, a fold change of 13.6 ± 2.3 in cell number compared to the seeding number was observed on cP*n*BA1100, whereas the fold change was 8.6 ± 0.5 on cP*n*BA250 (Figure 1C). Among the tested materials, TCP allowed the highest cell proliferation rate.

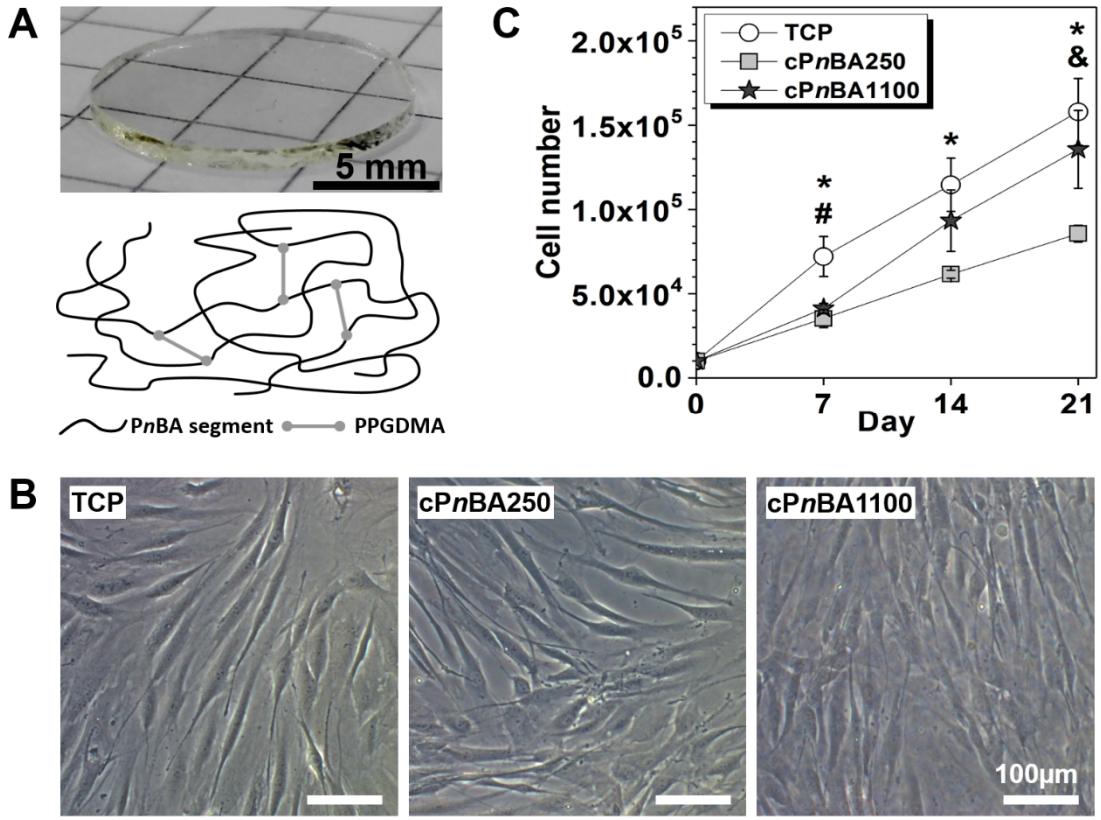

Figure 1. Adhesion and proliferation of hADSCs on TCP and cP*n*BA films. (A) Round-shaped cP*n*BA films with a diameter of 13 mm could be put into the commercial standard 24-well tissue culture plates for hADSC culture. The polymer contains P*n*BA segments crosslinked by PPGDMA. The mechanical properties of the films were tailored by changing the crosslinker amount. (B) Representative images showing early stage (24 hours) cell adhesion on cP*n*BA films and TCP. (C) Proliferation of hADSCs. The cell number was determined at indicated time points (n = 3, $p<0.05$ (*: TCP vs cP*n*BA250, #: TCP vs cP*n*BA1100, &: cP*n*BA250 vs cP*n*BA1100)).

3.2. Cell morphology and cytoskeleton

The morphology of MSCs and the structural organization of cytoskeletal filaments have been shown to be affected by elastic properties of the culturing materials. In general, MSCs contacted with a stiffer surface appeared more spread out than the cells on a softer material. Additionally, the F-actin stress fibers were stronger and better organized in the cells cultured on stiffer surface. Such a difference in cell morphology and cytoskeleton have been reported on softer gels with different stiffness (1-15 kPa) [25]

and on polymers with higher elastic moduli (0.1-310 MPa) [26]. Here, to study the structure and organization of cytoskeleton, the F-actin stress fibers and cell nuclei were stained after 2 weeks of culture on different materials (Figure 2A). Cells growing on TCP showed well orientated strong stress fibers. In contrast, relatively weak stress fibers were observed in cells on cP*n*BA250 and cP*n*BA1100 films. Further, the F-actin level was determined with an ELISA assay. In consistence with the fluorescence images in Figure 2A, the F-actin expression level on TCP was more than 2 times higher than on cP*n*BA films. In addition to the material surfaces, the different cell density on TCP and cP*n*BAs might lead to the different F-actin expression. It has been reported that the expression of integrin was dependent on the degree of cell confluence, although the patterns of change varied for some subunits [27]. Therefore, the cells on TCP, with a higher cell density as the result of higher proliferation rate, might present different integrin expression patterns from the cells on cP*n*BAs. This could further regulate the downstream F-actin expression. By comparing the cells on cP*n*BA250 and cP*n*BA1100, we did not observe a significant difference with respect to the structure, organization and expression level of F-actin (Figure 2B). This result might be due to that the difference of elastic modulus of these two cP*n*BA materials was not large enough to induce the changes of morphology and cytoskeleton in hADSCs. This observation after 2 weeks of culture was in consistence with the cell morphology 24 hours after cell seeding (Figure 1B), in which the cells presented the similar shape and size on cP*n*BA250 and cP*n*BA1100.

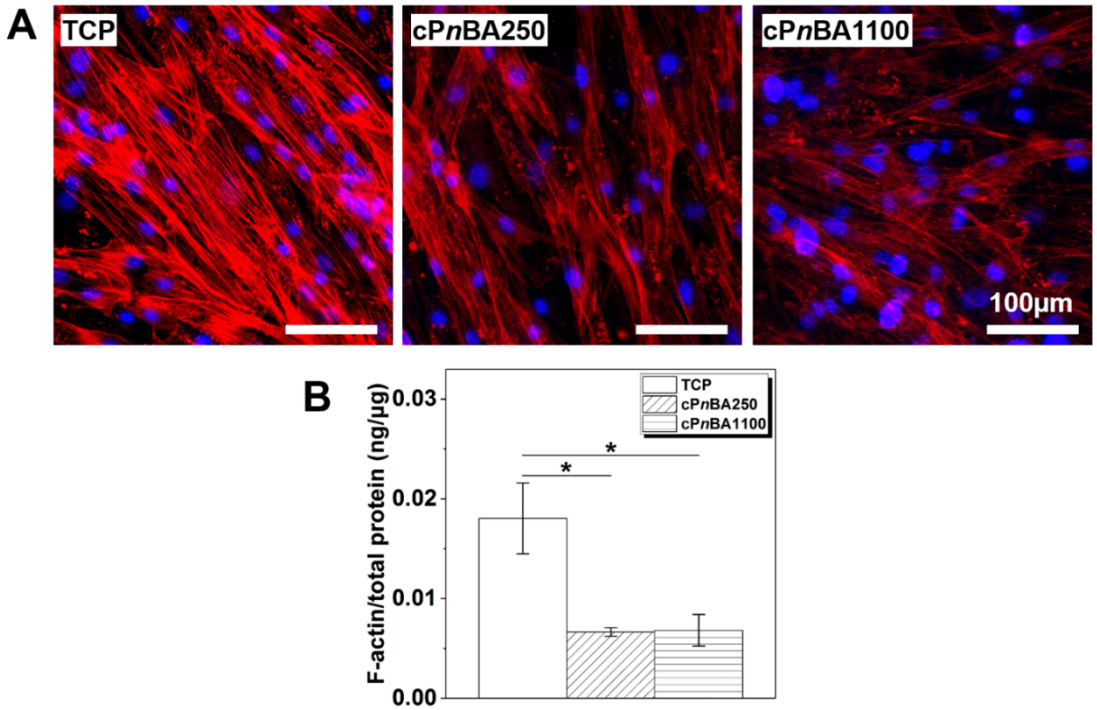

Figure 2. F-actin cytoskeletal structure and expression of hADSCs on TCP and cP*n*BA films. (A) Representative images of F-actin stress fibers (red) and cell nuclei (blue) staining after 2 weeks of culture. (B) F-actin amount in cells cultured on different materials for 2 weeks was determined with ELISA, and was normalized with the level of total cell protein. (n = 3, *$p < 0.05$).

3.3. Cell viability, apoptosis and cellular senescence

In order to evaluate the cytotoxicity of the materials, the live/dead staining experiment was performed (Figure 3A). After 2 weeks of culture, the cells were stained with FDA and PI to identify the living and dead cells respectively. Similar to the cells on TCP, the cells on both cP*n*BA films presented high viability and no dead cells were found, indicating a negligible cytotoxicity of the cP*n*BA polymers. This result is in line with our previous tests using different cell types, in which high cell viability was observed for L929 cells cultured in the extracts of cP*n*BAs [4] and primary endothelial cells cultured directly on cP*n*BA surface [5].

In addition to the induced cell death by cytotoxicity, the cells could undergo the programmed cell death, which is an intentional suicide termed apoptosis [28]. The

activation of caspase-3/7, a key biomarker of apoptosis, was determined to assess the cell apoptosis on different cP*n*BA films (Figure 3B). At day 1, the apoptosis was at a similar level in cells on different materials. After 1 week of culture, a higher level of apoptosis was observed in cells growing on cP*n*BA films, as compared to cells on TCP (36% (cP*n*BA250) and 33% (cP*n*BA1100) increase to TCP). The difference of mechanical properties between cP*n*BA250 and cP*n*BA1100 did not affect the cell apoptosis.

The function of MSCs could be also affected by cellular senescence, as a result of intrinsic events or external stimuli. Senescence may lead to a permanent cell cycle arrest, making MSCs lose their self-renewal capacity. In addition, the alteration of major functions of MSCs could occur with cellular senescence, including the differentiation potential, immunoregulatory capacity, migratory and homing ability [29,30]. The SA-ß-Gal, a biochemical marker of senescent cells, was therefore measured to evaluate the cellular senescence of hADSCs on different materials (Figure 3C). After 1 week of culture, a significantly lower senescence level was observed on cP*n*BA1100, as compared to TCP. After 3 weeks, the cellular senescence was at a similar level in all tested groups. Taken together, our results demonstrated the high cell compatibility of cP*n*BAs for hADSCs, with respect to the cell viability, apoptosis and cellular senescence.

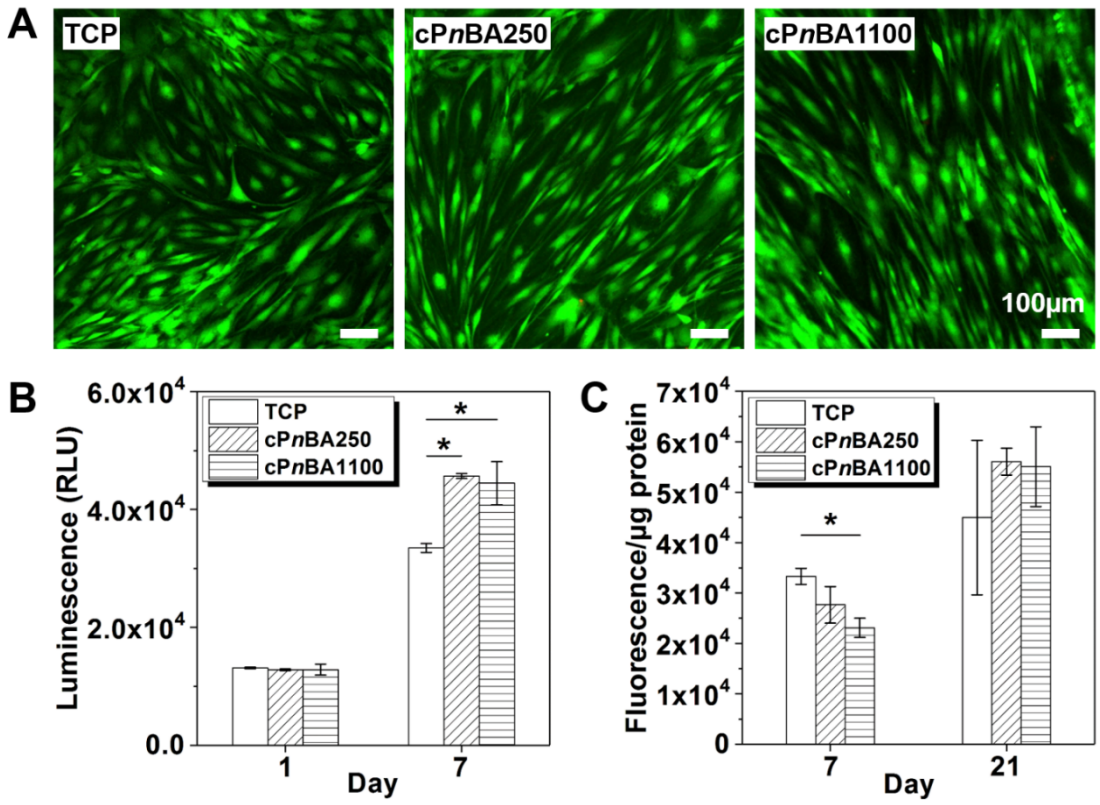

Figure 3. (A) Representative images of live/dead staining of hADSCs with FDA (green) and PI (red) after 2 weeks of culture. (B) The cell apoptosis was evaluated by detecting the activation of caspase-3/7. (C) The level of cellular senescence was assessed by measuring the activity of the acidic senescence associated β-galactosidase. (n = 3; $*p < 0.05$)

3.4. Inflammatory cytokine secretion

As the sensor and switcher of inflammation, MSCs own the function of immune-modulation. They could exert either a pro-inflammatory or an anti-inflammatory effect through the direct cell-cell contacts and/or secretion of multiple inflammatory cytokines [31,32]. Previous studies have suggested that the secretion profile of MSCs could be regulated by the properties of cell culturing materials, such as the surface structure [33] and the substrate elasticity (ranging from 2 to 20 kPa) [34]. Therefore, the levels of secreted inflammatory cytokines were recorded up to 3 weeks in this study to investigate the influence of cP*n*BA elasticity on immunomodulatory capability of hADSCs (Figure 4).

At day 21, cells on cP*n*BA1100 expressed a lower level of interleukin-6 (IL-6) than on TCP. Similar results were observed for pro-inflammatory interleukin-8 (IL-8) at day 7 and 14, monocyte chemoattractant protein 1 (MCP-1) at day 1 and 7, as well as anti-inflammatory interleukin-1 receptor antagonist (IL-1Ra) at day 7. No huge difference was observed for pro-inflammatory cytokines tumor necrosis factor alpha (TNFα) and interferon gamma (IFNγ). Taking all the data together, our results demonstrated that the difference of elasticity between cP*n*BA250 and cP*n*BA1100 did not show dramatic influence on secretion of inflammatory cytokines in hADSCs. The cP*n*BA polymers did not induce marked alteration in hADSC secretion profile as compared to TCP.

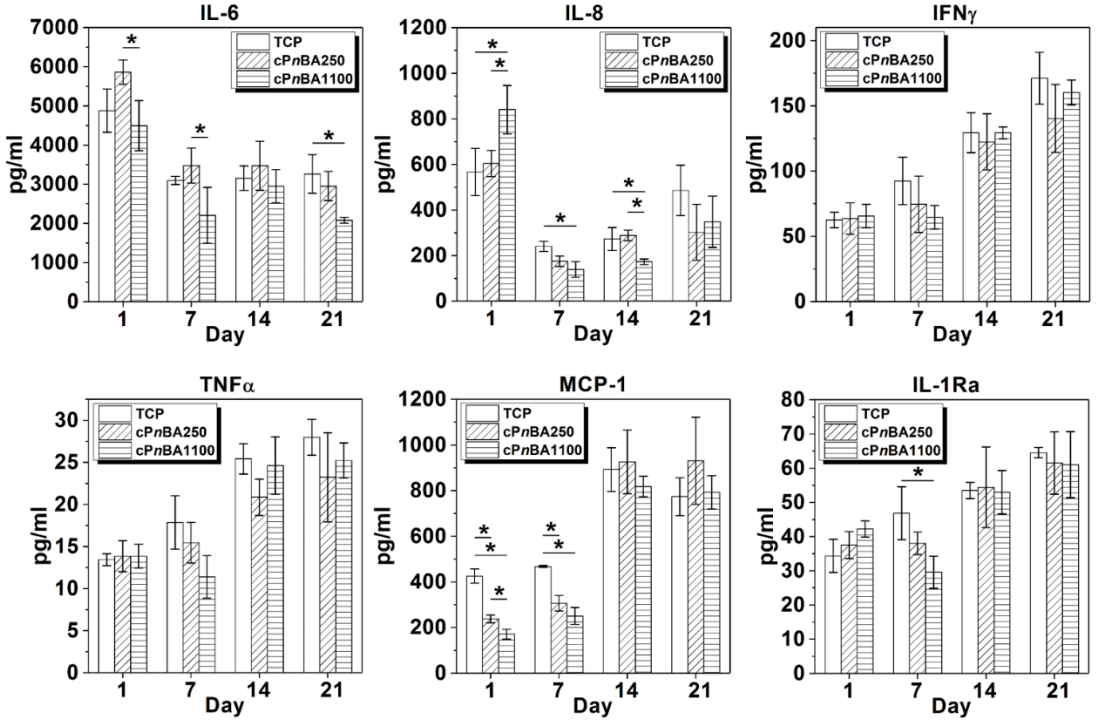

Figure 4. Secretion of inflammatory cytokines of hADSCs growing on TCP and cP*n*BA films. The concentration of cytokines in the conditioned medium was measured using a Bio-Plex 200 system. (n = 3, *$p < 0.05$)

3.5. VEGF expression and cell migration

The secretome of MSCs has emerged as an effective and safe therapeutic for treatment of a variety of diseases. As a cell free therapeutic, MSC secretome can promote angiogenesis and stimulate tissue adjacent cells and endogenous stem cells [35,36].

Among the complex constituents of MSC secretome, VEGF is the major growth factor contributing to angiogenesis, which serves as the predominant inducer and mediator during angiogenic processes [37-39]. VEGF can stimulate proliferation and migration of endothelial cells located in pre-existing blood vessels to form new blood vessel sprouts, which is then anastomosis with each other to form the tubular-like vascular structures [40]. Further, VEGF can mobilize endothelial progenitor cells to the injury site, where they differentiate into mature endothelial cells and contribute to neovessel formation. The MSCs have been considered as a stable source of VEGF production, which is of great importance to improve the endothelialization and long-term patency of MSC-based artificial blood vessels. The VEGF secretion profile of hADSCs on different materials was assessed up to 3 weeks in this study (Figure 5). At day 1, cells on TCP and cP*n*BA250 exhibited the higher level of VEGF expression than on cP*n*BA1100. Markedly, from day 7 to day 21, the VEGF secretion was induced by cP*n*BA250 to a significant level, which was around 2 times as high as that in cP*n*BA1100 and TCP cultures. This result suggested that cP*n*BA250 might be superior to cP*n*BA1100 for promoting pro-angiogenic capacity of MSCs. The mechanism for enhanced VEGF secretion on cP*n*BA250 might involve the integrin-mediated signaling pathways [15] as well as the stimulation of pro-inflammatory cytokines such as IL-6 [41], which need to be clarified in the future studies.

Previous reports have shown that the migration of MSCs could be promoted by VEGF [42,43]. The process of VEGF-induced MSC migration involved the promotion of focal adhesion formation and cytoskeletal rearrangement [44,45]. Based on the significantly enhanced VEGF secretion of hADSCs on cP*n*BA250, we then evaluated the motility of cells on different materials after 2 days of culture, via recording the random cell movement for 24 hours using a time-lapse microscope. As expected, the hADSCs could freely move on all tested materials, with the fastest migration on cP*n*BA250 surface (Figure 6A). The migration velocity of hADSCs on cP*n*BA250 (0.70 ± 0.03 μm/min) was 78% and 157% higher than on TCP (0.39 ± 0.02 μm/min) and on cP*n*BA1100 (0.27

± 0.02 μm/min), respectively (Figure 6B). This observation was in consistence with the increased VEGF secretion of hADSCs on cP*n*BA250 film.

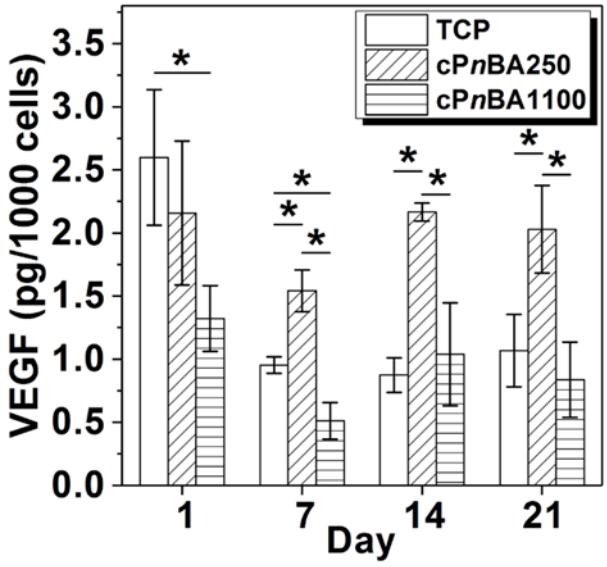

Figure 5. VEGF secretion of hADSCs on TCP and cP*n*BA films. The VEGF in the conditioned medium was quantified with ELISA assay, and was normalized with cell number. (n = 3; $*p < 0.05$)

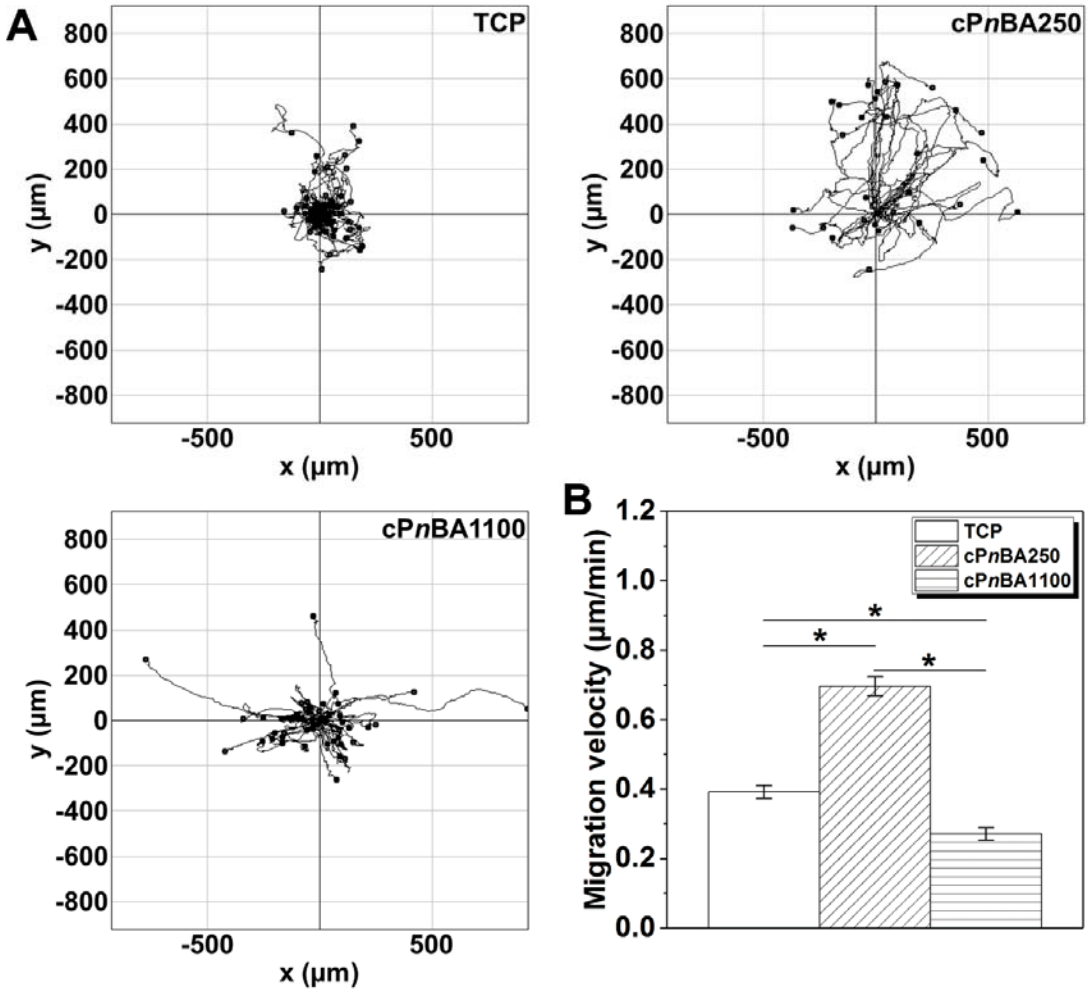

Figure 6. Migration of hADSCs on TCP and cP*n*BA films. After 2 days of culture, the cell nuclei were stained with Hoechst 33342 and were tracked up to 24 hours with a time-lapse microscope to generate the trajectories (A) and quantify the migration velocity (B). (Mean ± SEM; n ≥ 29; ∗p <0.05)

4. Conclusion

Aiming to investigate the influence of scaffold elasticity in the range of native arteries on the cellular behavior and function of MSCs, we cultured hADSCs on cP*n*BA films with Young's modulus of 250 kPa and 1100 kPa. Both cP*n*BA polymer networks presented high cell compatibility for hADSC culture. They did not show cytotoxicity to the cells, and allowed high cell attachment as well as long-term proliferation. The cell morphology, cytoskeleton assembly, apoptosis and cellular senescence of hADSCs

were not markedly affected by the elasticity of tested cP*n*BA polymers. Compared to cP*n*BA250, a higher cell proliferation rate was observed on cP*n*BA1100. Notably, the pro-angiogenic capacity of hADSCs was enhanced by cP*n*BA250 substrate. The VEGF secretion activity of cells on cP*n*BA250 was significantly higher than on cP*n*BA1100, suggesting that culture of MSCs on cP*n*BA250 might promote the endothelialization process. Taken together, our results demonstrated the high potential of cP*n*BA polymer networks as synthetic vascular grafts for constructing stem cell-based artificial blood vessels. Tuning the elastic profile of the polymer scaffolds to regulate stem cells might be an effective strategy to improve the endothelialization and long-term engraftment of vascular prosthesis, which are of great importance to the function and clinical benefit of artificial blood vessels.

5. Acknowledgements

This work was financially supported by the Helmholtz Association of German Research Centers (Helmholtz-Portfolio Topic “Technology and Medicine”, Helmholtz Virtual Institute “Multifunctional Biomaterials for Medicine” (VH-VI-423), and programme-oriented funding) and the German Federal Ministry of Education and Research (BMBF project number 0315696A “Poly4Bio BB”).

References

[1] Zhang WJ, Liu W, Cui L and Cao YL. Tissue engineering of blood vessel, J Cell Mol Med 2007; 11(5): 945-957.

[2] Pankajakshan D and Agrawal DK. Scaffolds in tissue engineering of blood vessels, Can J Physiol Pharm 2010; 88(9): 855-873.

[3] Anadol R and Gori T. The mechanisms of late scaffold thrombosis, Clin Hemorheol Micro 2017; 67(3-4): 343-346.

[4] Cui J, Kratz K, Hiebl B, Jung F and Lendlein A. Soft poly(n-butyl acrylate) networks with tailored mechanical properties designed as substrates for in vitro models, Polym Advan Technol 2011; 22(1): 126-132.

[5] Hiebl B, Cui J, Kratz K, Frank O, Schossig M, Richau K, Lee S, Jung F and Lendlein A. Viability, Morphology and Function of Primary Endothelial Cells on Poly(n-Butyl Acrylate) Networks Having Elastic Moduli Comparable to Arteries, J Biomat Sci-Polym E 2012; 23(7): 901-915.

[6] Roch T, Cui J, Kratz K, Lendlein A and Jung F. Immuno-compatibility of soft hydrophobic poly(n-butyl acrylate) networks with elastic moduli for regeneration of functional tissues, Clin Hemorheol Micro 2012; 50(1-2): 131-142.

[7] Lee HY and Oh BH. Aging and Arterial Stiffness, Circ J 2010; 74(11): 2257-2262.

[8] Patel DJ and Janicki JS. Static elastic properties of the left coronary circumflex artery and the common carotid artery in dogs, Circulation research 1970; 27(2): 149-58.

[9] Riley WA, Barnes RW, Evans GW and Burke GL. Ultrasonic Measurement of the Elastic-Modulus of the Common Carotid-Artery - the Atherosclerosis Risk in Communities (Aric) Study, Stroke 1992; 23(7): 952-956.

[10] Hsia K, Yao CL, Chen WM, Chen JH, Lee H and Lu JH. Scaffolds and Cell-Based Tissue Engineering for Blood Vessel Therapy, Cells Tissues Organs 2015; 202(5-6): 281-295.

[11] Nemeno-Guanzon JG, Lee S, Berg JR, Jo YH, Yeo JE, Nam BM, Koh YG and Lee JI. Trends in Tissue Engineering for Blood Vessels, J Biomed Biotechnol 2012: doi: 10.1155/2012/956345.

[12] Thomas H, Cowin AJ and Mills SJ. The Importance of Pericytes in Healing: Wounds and other Pathologies, Int J Mol Sci 2017; 18(6): doi: 10.3390/ijms18061129.

[13] Bergers G and Song S. The role of pericytes in blood-vessel formation and maintenance, Neuro-Oncology 2005; 7(4): 452-464.

[14] Du J, Chen XF, Liang XD, Zhang GY, Xu J, He LR, Zhan QY, Feng XQ, Chien S and Yang C. Integrin activation and internalization on soft ECM as a mechanism of induction of stem cell differentiation by ECM elasticity, P Natl Acad Sci USA 2011; 108(23): 9466-9471.

[15] Li ZD, Wang WW, Xu X, Kratz K, Zou J, Lysyakova L, Heuchel M, Kurtz A, Gossen M, Ma N and Lendlein A. Integrin beta 1 activation by micro-scale

curvature promotes pro-angiogenic secretion of human mesenchymal stem cells, J Mater Chem B 2017; 5(35): 7415-7425.
[16] Xu BY, Song GB, Ju Y, Li X, Song YH and Watanabe S. RhoA/ROCK, cytoskeletal dynamics, and focal adhesion kinase are required for mechanical stretch-induced tenogenic differentiation of human mesenchymal stem cells, J Cell Physiol 2012; 227(6): 2722-2729.
[17] D'Angelo F, Tiribuzi R, Armentano I, Kenny JM, Martino S and Orlacchio A. Mechanotransduction: tuning stem cells fate, J Funct Biomater 2011; 2(2): 67-87.
[18] Han FX, Zhu CH, Guo QP, Yang HL and Li B. Cellular modulation by the elasticity of biomaterials, J Mater Chem B 2016; 4(1): 9-26.
[19] Engler AJ, Sen S, Sweeney HL and Discher DE. Matrix elasticity directs stem cell lineage specification, Cell 2006; 126(4): 677-689.
[20] Xu X, Wang WW, Kratz K, Fang L, Li ZD, Kurtz A, Ma N and Lendlein A. Controlling Major Cellular Processes of Human Mesenchymal Stem Cells using Microwell Structures, Adv Healthc Mater 2014; 3(12): 1991-2003.
[21] Harburger DS and Calderwood DA. Integrin signalling at a glance, J Cell Sci 2009; 122(2): 159-163.
[22] Shattil SJ, Kim C and Ginsberg MH. The final steps of integrin activation: the end game, Nat Rev Mol Cell Bio 2010; 11(4): 288-300.
[23] Sun MY, Chi GF, Li PD, Lv S, Xu JJ, Xu ZR, Xia YH, Tan Y, Xu JY, Li LS and Li YL. Effects of Matrix Stiffness on the Morphology, Adhesion, Proliferation and Osteogenic Differentiation of Mesenchymal Stem Cells, Int J Med Sci 2018; 15(3): 257-268.
[24] Wang LS, Boulaire J, Chan PPY, Chung JE and Kurisawa M. The role of stiffness of gelatin-hydroxyphenylpropionic acid hydrogels formed by enzyme-mediated crosslinking on the differentiation of human mesenchymal stem cell, Biomaterials 2010; 31(33): 8608-8616.
[25] Park JS, Chu JS, Tsou AD, Diop R, Tang ZY, Wang AJ and Li S. The effect of matrix stiffness on the differentiation of mesenchymal stem cells in response to TGF-beta, Biomaterials 2011; 32(16): 3921-3930.
[26] Olivares-Navarrete R, Lee EM, Smith K, Hyzy SL, Doroudi M, Williams JK, Gall K, Boyan BD and Schwartz Z. Substrate Stiffness Controls Osteoblastic and Chondrocytic Differentiation of Mesenchymal Stem Cells without Exogenous Stimuli, PLoS One 2017; 12(1): e0170312.
[27] Stanley AJ, Banks RE, Southgate J and Selby PJ. Effect of Cell-Density on the Expression of Adhesion Molecules and Modulation by Cytokines, Cytometry 1995; 21(4): 338-343.
[28] Majno G and Joris I. Apoptosis, Oncosis, and Necrosis - an Overview of Cell-Death, Am J Pathol 1995; 146(1): 3-15.
[29] Li Y, Wu Q, Wang YJ, Li L, Bu H and Bao J. Senescence of mesenchymal stem cells, Int J Mol Med 2017; 39(4): 775-782.

[30] Turinetto V, Vitale E and Giachino C. Senescence in Human Mesenchymal Stem Cells: Functional Changes and Implications in Stem Cell-Based Therapy, Int J Mol Sci 2016; 17(7), E1164.
[31] Bernardo ME and Fibbe WE. Mesenchymal Stromal Cells: Sensors and Switchers of Inflammation, Cell Stem Cell 2013; 13(4): 392-402.
[32] Kyurkchiev D, Bochev I, Ivanova-Todorova E, Mourdjeva M, Oreshkova T, Belemezova K and Kyurkchiev S. Secretion of immunoregulatory cytokines by mesenchymal stem cells, World J Stem Cells 2014; 6(5): 552-70.
[33] Leuning DG, Beijer NRM, du Fosse NA, Vermeulen S, Lievers E, van Kooten C, Rabelink TJ and de Boer J. The cytokine secretion profile of mesenchymal stromal cells is determined by surface structure of the microenvironment, Sci Rep-Uk 2018; 87716.
[34] Seib FP, Prewitz M, Werner C and Bornhauser M. Matrix elasticity regulates the secretory profile of human bone marrow-derived multipotent mesenchymal stromal cells (MSCs), Biochem Bioph Res Co 2009; 389(4): 663-667.
[35] Kim HO, Choi SM and Kim HS. Mesenchymal Stem Cell-Derived Secretome and Microvesicles as a Cell-Free Therapeutics for Neurodegenerative Disorders, Tissue Eng Regen Med 2013; 10(3): 93-101.
[36] Caplan AI and Dennis JE. Mesenchymal stem cells as trophic mediators, J Cell Biochem 2006; 98(5): 1076-1084.
[37] Lee EJ, Park HW, Jeon HJ, Kim HS and Chang MS. Potentiated therapeutic angiogenesis by primed human mesenchymal stem cells in a mouse model of hindlimb ischemia, Regen Med 2013; 8(3): 283-293.
[38] Hoeben A, Landuyt B, Highley MS, Wildiers H, Van Oosterom AT and De Bruijn EA. Vascular endothelial growth factor and angiogenesis, Pharmacol Rev 2004; 56(4): 549-580.
[39] Boomsma RA and Geenen DL. Mesenchymal Stem Cells Secrete Multiple Cytokines That Promote Angiogenesis and Have Contrasting Effects on Chemotaxis and Apoptosis, Plos One 2012; 7(4): e35685.
[40] Salha S, Gehmert S, Brebant V, Anker A, Loibl M, Prantl L and Gehmert S. PDGF regulated migration of mesenchymal stem cells towards malignancy acts via the PI3K signaling pathway, Clin Hemorheol Microcirc 2018, doi: 10.3233/CH-189319.
[41] Maloney JP and Gao L. Proinflammatory Cytokines Increase Vascular Endothelial Growth Factor Expression in Alveolar Epithelial Cells, Mediat Inflamm 2015, 387842.
[42] Ball SG, Shuttleworth CA and Kielty CM. Vascular endothelial growth factor can signal through platelet-derived growth factor receptors, J Cell Biol 2007; 177(3): 489-500.
[43] Beckermann BM, Kallifatidis G, Groth A, Frommhold D, Apel A, Mattern J, Salnikov AV, Moldenhauer G, Wagner W, Diehlmann A, Saffrich R, Schubert M, Ho AD, Giese N, Buchler MW, Friess H, Buchler P and Herr I. VEGF expression by mesenchymal stem cells contributes to angiogenesis in pancreatic carcinoma, Brit J Cancer 2008; 99(4): 622-631.

[44] Ke CH, Chen JA, Guo YJ, Chen ZW and Cai JY. Migration mechanism of mesenchymal stem cells studied by QD/NSOM, Bba-Biomembranes 2015; 1848(3): 859-868.
[45] Wang HH, Wang XK, Qu J, Yue Q, Hu YN and Zhang HX. VEGF Enhances the Migration of MSCs in Neural Differentiation by Regulating Focal Adhesion Turnover, J Cell Physiol 2015; 230(11): 2728-2742.